2007 IEEE International Conference on
Robotics and Automation
Roma, Italy, 10-14 April 2007

Flexible Force Control for Accurate Low-Cost Robot Drilling

Tomas Olsson, Anders Robertsson, Rolf Johansson
Department of Automatic Control, LTH, Lund University,
SE-221 00 Lund, Sweden
E-mail: tomas.olsson@control.lth.se

***Abstract*— The problem of robot drilling presents a significant challenge, due to the comparatively low mechanical stiffness of typical serial industrial robots. This compliance makes the robot deflect due to the cutting forces, resulting in poor hole quality. Recently, functionality for high-bandwidth force control has found its way into industrial robot control systems. This could potentially open up the possibility of robotic drilling systems with improved performance, using only standard systems without costly extra hardware and calibration techniques. In this paper, we present methods and systems for force-controlled robot drilling, based on active suppression of drill sliding through a model-based force control scheme. The methods are validated in a number of drilling experiments using an industrial robot.**

I. Introduction

Systems for automatic drilling have a long history both in industry and the research community. In particular, the use of industrial robots for drilling is interesting due to their flexible programming and the comparatively low cost of industrial robot systems. However, robot drilling is a very challenging task due to the comparatively low mechanical stiffness of the typical serial industrial robots in use today. This compliance makes the robot deflect due to the cutting forces, with poor hole quality as a result. Nevertheless, a number of industrial robot systems for drilling exist. Traditionally, such systems have been based on mechanical solutions, using heavy robots and customized, high-cost drilling end-effectors. In addition, different devices for rigidly attaching the drilling tool to the surface are commercially available, for instance, based on vacuum suction or electromagnetic devices. In many situation, such devices provide very robust solutions, although somewhat inflexible.

In many drilling tasks, for example in aircraft construction, components consisting of several layers of material are drilled. In such cases, it is important to simultaneously apply pressure to the surface in order to make sure that no chips or other material from the drilling are lodged between the layers, in which case the entire structure would have to be manually disassembled and cleaned. The pressure force which is applied must therefore be controlled during the entire drilling phase, which makes high-bandwidth feedback techniques an attractive alternative to mechanical solutions. Research and development on force-controlled drilling has not received as much attention as many other applications of industrial force control, such as assembly, deburring, milling or polishing. The reason is probably the difficulties involved in robotic drilling, as well as the lack of available industrial robot systems with capacity for sufficiently high-bandwidth force control. Some results on force control for special drilling machines have been reported in [1]. Experimental systems for force-controlled robot drilling have been presented in [2], where a force controller with inner-loop position control was used for the drilling thrust force control, and in [3], where an application to bone drilling in orthopedic surgery was presented. In addition, numerous research papers and patents related to robot drilling exist, which are based on mechanical solutions or special-purpose end-effectors rather than force control.

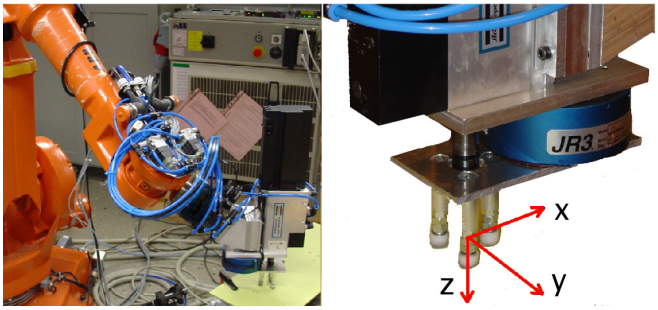

Fig. 1. Robot, drilling tool and tripod, with JR3 force sensor mounted on the drilling tool. As seen in the figure, the axial direction is denoted z, while the x- and y-directions are tangential to the surface during drilling.

The purpose of this paper is to develop and evaluate techniques for force control using an industrial robot setup, shown in Fig. 1. The setup consists of a robot holding a pneumatic drilling tool equipped with a pressure foot in the form of a tripod. The goal is to apply a constant normal force to the drilled surface with the tripod prior to drilling, and to keep the tangential forces small enough to avoid sliding of the drilling tool on the surface during drilling. The undesired sliding is due to the compliance in the robot transmission, links and environment, and could be up to several millimeters without compensation, seriously degrading both quality and positioning of drilled holes. The proposed solution is based on a combination of high-bandwidth control of the axial forces applied to the workpiece, and active suppression of the sliding forces through a model-based force control scheme. The forces are measured using a stiff six-axis force/torque sensor, mounted directly between the drilling machine and the tripod, see Fig. 1. A separate, pneumatically driven axis of the drilling machine feeds the drill along the tripod central axis and into the material. The feasibility of the proposed method is demonstrated in drilling experiments using an industrial robot system.

1-4244-0602-1/07/$20.00 ©2007 IEEE.

II. Modeling and Control

The external force control interface exploits the existing inner motion control structure of the robot system, extended to include the possibility for external actuation through changing joint-level servo motion references at a 4 ms sampling time [4]. For the purposes of simulation and model-based control design, a dynamic model of the system responses to external forces and motion references is required. In order to illustrate the expected properties of such a model, a local model is assumed in the form

$$\mathbf{M}_a\ddot{\mathbf{p}}_a+\mathbf{D}_1\dot{\mathbf{p}}_a+\mathbf{K}\mathbf{p}_a=\mathbf{K}\mathbf{p}_m+\mathbf{D}_2\dot{\mathbf{p}}_m+\mathbf{f}_e \quad (1)$$

$$\mathbf{M}_m\ddot{\mathbf{p}}_m+\mathbf{D}_3\dot{\mathbf{p}}_m+\mathbf{K}\mathbf{p}_m=\mathbf{K}\mathbf{p}_a+\mathbf{D}_4\dot{\mathbf{p}}_a+\mathbf{f}_c \quad (2)$$

where $\mathbf{p}_m$ and $\mathbf{p}_a$ are the motor and arm side positions in local Cartesian coordinates, and $\mathbf{f}_c$ and $\mathbf{f}_e$ are the (transformed) control torque and external force on the tool, respectively. $\mathbf{M}_a$ and $\mathbf{M}_m$ represent the arm and motor inertias, $\mathbf{D}_i$ are damping matrices and $\mathbf{K}$ represent elasticity in the transmission and links. Together with a feedback/feedforward type motion controller

$$\mathbf{f}_c=-\mathbf{f}_{\text{fb}}(\mathbf{p}_m,\dot{\mathbf{p}}_m)+\mathbf{f}_{\text{ff}}(\mathbf{p}_r,\dot{\mathbf{p}}_r)+\mathbf{f}_I\left(\int \mathbf{p}_r-\mathbf{p}_m dt\right)+\mathbf{f}_{\text{ffw}} \quad (3)$$

it leads to a full model of the motion-controlled robot. The position/velocity signals $\mathbf{p}_r$ and $\dot{\mathbf{p}}_r$, corresponding to the references for the inner motion controllers, are the control inputs to be used by the external control. In the presence of a constant non-zero external disturbance force $\mathbf{f}_e=\mathbf{f}_0$ and zero reference $\mathbf{p}_r=0$, in stationarity we obtain the equilibrium

$$\mathbf{p}_m=\mathbf{0} \quad (4)$$

$$\mathbf{p}_a=\mathbf{K}^{-1}\mathbf{f}_0. \quad (5)$$

As the Cartesian stiffness matrix $\mathbf{K}$ will in general not be diagonal, this means that the deflection in the tool position will not be in the direction of the external force. In particular, the axial forces on the drill and pressure foot will make the robot bend and deflect tangentially to the surface, causing a sliding motion which must be compensated for.

The model in Eqs. (1)–(3) was the basis for a tuned model used for control design. By exploiting the special structure of the Eqs. (1)–(3) and a typical robot motion controller structure, models that capture the behavior of the controlled robot were experimentally obtained. In order to obtain better reliability, the tuning procedure was divided into a static and a dynamic step. In the first stage, an algorithm for static calibration was used to find the stiffness matrix $\mathbf{K}$. In the second stage of the tuning, a dynamic model including the motion-controlled rigid robot dynamics, resonances, and couplings between the motion directions was tuned, given motion references $\mathbf{p}_r$ and external tool forces $\mathbf{f}_e$ as inputs. A pseudo-random binary excitation signal was sent as a motion reference to the unconstrained robot, and both motor- and arm side positions were measured. A discrete-time input-output model of the arm side motion was found

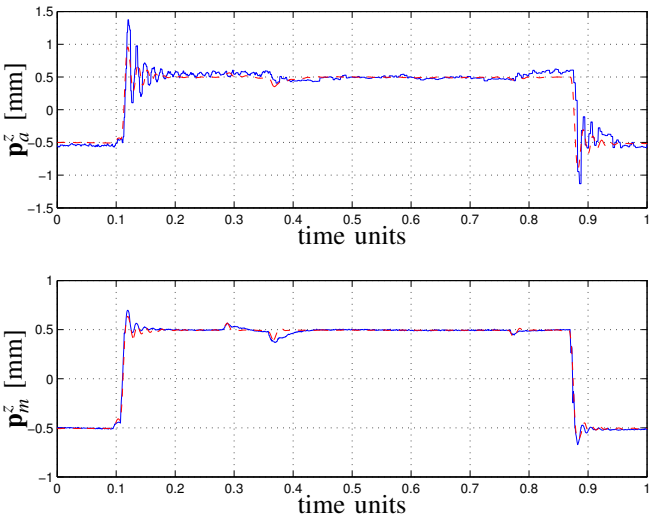

Fig. 2. True arm side (top) and motor side (bottom) reference step responses (solid lines) in the z-direction, and the corresponding step responses of the model obtained by the tuning procedure (dashed lines). A modified and aggressively tuned velocity feedforward, in combination with the increased flexibility represented by the drilling tool, gave a faster and more resonant response to motion references than the built-in controllers.

by minimizing the quadratic criterion

$$J(\bar{\mathbf{A}},\bar{\mathbf{B}},\bar{\mathbf{F}},\bar{\mathbf{G}},\bar{\mathbf{H}})=\sum_{k=n_a}^{N}\left[\sum_{j=0}^{n_a}\left(\bar{\mathbf{A}}_j\mathbf{p}_a(k-j)\right)-\bar{\mathbf{B}}\mathbf{p}_m(k-1)+\right.$$
$$\left.+\sum_{j=0}^{n_m}\left(\bar{\mathbf{F}}_j\mathbf{p}_m(k-j)\right)-\sum_{i=1}^{z_m+1}\left(\bar{\mathbf{G}}_i\mathbf{p}_a(k-i)\right)-\bar{\mathbf{H}}\mathbf{p}_r(k-1)\right]^2 \quad (6)$$

subject to the constraints

$$\bar{\mathbf{B}}=\sum_{k=0}^{n_a}\bar{\mathbf{A}}_k,\quad \sum_{k=0}^{n_m}\bar{\mathbf{F}}_k=\bar{\mathbf{H}},\quad \sum_{k=1}^{z_m+1}\bar{\mathbf{G}}_k=\mathbf{0} \quad (7)$$

stating the physical property that the system was statically decoupled by the integral action, giving a system with unit static gain. For validation of the obtained model, the true reference step responses were compared to the step responses predicted by the obtained model. The resulting reference step responses for a 3-degree-of-freedom model of translation only can be seen in Fig. 2, and the true and simulated arm side responses to an external force $\mathbf{f}_e$ can be seen in Fig. 3. A good fit was obtained both statically and around the resonance frequencies.

During stiction contact between the tripod and the drilled component, the contact behavior was similar to a very stiff and poorly damped spring, as predicted by many friction models such as the LuGre model [5]. When the tangential forces became larger than the break-away forces of the stiction, the tripod started to slide across the surface, with poor hole quality and positioning as a result. Therefore, it was important both to control the tangential forces so that sliding was avoided, and to control the moments to keep the tripod in contact with the surface at each of the three contact points. Once such a contact had been achieved, the dependence of the contact force $\mathbf{f}_e$ on the tool position $\mathbf{p}_a$ was expressed

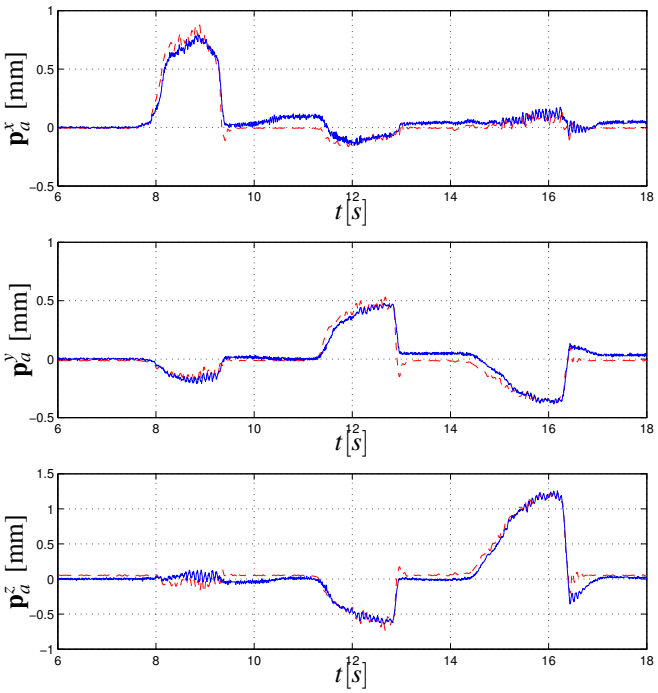

Fig. 3. True arm side external force responses (solid lines) in the x-, y- and z-directions, and the corresponding responses of the model obtained by the tuning procedure (dashed lines)

through the environmental dynamics. The resulting high-gain feedback loop affected the stability and performance of the manipulator. For a point contact, the environment dynamics can often be approximated by a local stiffness, or as a (non-linear) spring-damper [6]. For the tripod contact of the drilling tool used in this work, it was necessary to take also the geometry of the contact into account. The contact was considered as a combination of three-point contacts, where the force acting at each point contributed to the effective force and moment acting at the robot TCP point. General frameworks for multi-contact situations have previously been demonstrated, e.g., in [7] using an operational space formulation. In the drilling application, using a position/velocity-controlled robot, the contact properties of the small tripod could be expressed as a (non-diagonal) stiffness matrix. For the model of the 5-DoF system used in the experiments, the tool position $\mathbf{p}_a = \begin{bmatrix}\mathbf{t}_a^T & \varphi_{a,x} & \varphi_{a,y}\end{bmatrix}^T$ was represented by the three translations $\mathbf{t}_a$ and the two rotation angles $\varphi_{a,x}$ and $\varphi_{a,y}$ around the x- and y-axes (see Fig. 1), expressed in a fixed coordinate system which was taken to coincide with the initial position of the tool, $\mathbf{p}_a = \mathbf{0}$. The coordinates $\mathbf{X}_i^w$ of each contact point in the world coordinate system were related to $\mathbf{p}_a$ by

$$\mathbf{X}_i^w = \mathbf{R}_x(\varphi_{a,x})\mathbf{R}_y(\varphi_{a,y})\mathbf{X}_i^{TCP} + \mathbf{t}_a \approx \approx \begin{bmatrix} 1 & 0 & 0 & 0 & \mathbf{z}_i^{TCP} \\ 0 & 1 & 0 & -\mathbf{z}_i^{TCP} & 0 \\ 0 & 0 & 1 & \mathbf{y}_i^{TCP} & -\mathbf{x}_i^{TCP} \end{bmatrix} \mathbf{p}_a \stackrel{\text{def.}}{=} \mathscr{X}_i \mathbf{p}_a \quad (8)$$

where $\mathbf{X}_i^{TCP} = \begin{bmatrix}\mathbf{x}_i^{TCP} & \mathbf{y}_i^{TCP} & \mathbf{z}_i^{TCP}\end{bmatrix}$ describes the TCP-coordinates of the contact points of the tripod. Assuming a linear stiffness $\mathbf{f}_i = \mathbf{K}_i \mathbf{X}_i^w$ at each contact point, the full contact stiffness model was given by

$$\mathbf{f}_e = \sum_{i=1}^{3} \left(\begin{bmatrix} \mathbf{K}_i \mathscr{X}_i \\ \text{skew}(\mathbf{X}_i^{TCP}) \mathbf{K}_i \mathscr{X}_i \end{bmatrix} \right) \mathbf{p}_a \stackrel{\text{def.}}{=} \mathbf{K}_e \mathbf{p}_a \quad (9)$$

with the skew-symmetric matrix $\text{skew}(\mathbf{x}) = -\text{skew}(\mathbf{x})^T$ representing the cross-product, $\text{skew}(\mathbf{x})\mathbf{y} = \mathbf{x} \times \mathbf{y}$. For the setup described in this work, where the contact points were placed symmetrically on a circle in the xy-plane with radius r around the origin, and where each point stiffness matrix $\mathbf{K}_i = \text{diag}(k_x, k_y, k_z)$ was assumed to be completely decoupled, the contact model was also decoupled with stiffness matrix

$$\mathbf{K}_e = \text{diag}(3k_x, 3k_y, 3k_z, 1.5r^2k_z, 1.5r^2k_z). \quad (10)$$

The contact model in Eq. (9) provided a useful local approximation during stiction, and the objective of the control was to keep the system in this stiction regime.

A. Control Design

In the control design it is necessary to take both robot dynamics and environment properties into account. Therefore, in addition to the model-based control, the option to tune controllers manually in order to account for poorly modeled or varying environment parameters is desired. Automatic design procedures for force controllers have previously been presented [8], but they are not suitable for the drilling application due to the significantly higher contact stiffness and special control objectives. Instead, we propose a control strategy based on an easily tunable force controller using an inner motion controller with model-based disturbance rejection and decoupling. In inner-motion force control, the measured contact force and force reference are used as inputs in the integration of a motion- or impedance equation. This relation is often chosen as a passive second-order system in order to emulate the behavior of a passive mass-spring-damper. The robot motion controller is set to track the output position from the impedance equation. Because of the limited bandwidth of the motion control system and the deformations of the robot caused by external forces, the tracking of the desired motion may be poor when the robot is in contact with a stiff environment.

In order to improve the tracking performance, it was possible to redesign the inner motion control to include external force compensation. This can be seen as trying to increase the "stiffness" of the robot as seen from the tool, which improves the ability to control contact forces and moments. We used a controller structure which includes this inner loop compensation as in Fig. 4. In order to track the desired position obtained by integrating the impedance relation, the inner motion controller should have both a fast arm side response to motion commands, and good suppression of external forces up to the desired bandwidth of the system. In addition to force sensors, which can be used to obtain improved disturbance suppression through feedforward, feedback from arm side position measurements could be used in the inner controller to improve the *absolute* accuracy of the positioning. Such measurements could be

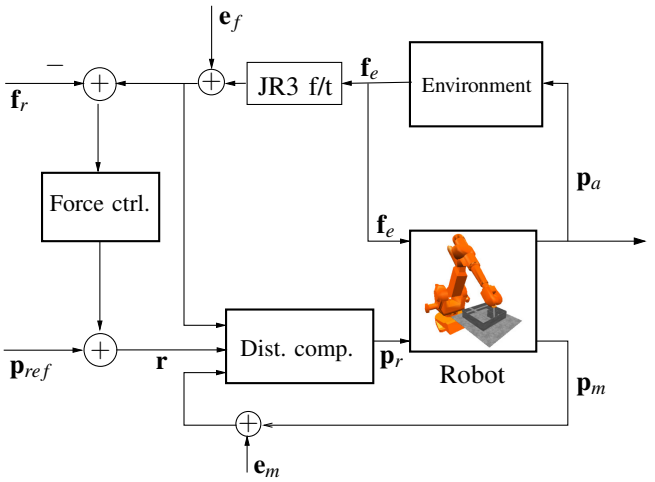

Fig. 4. Simplified structure of the control system for drilling, with an outer force control loop and inner-loop disturbance compensation.

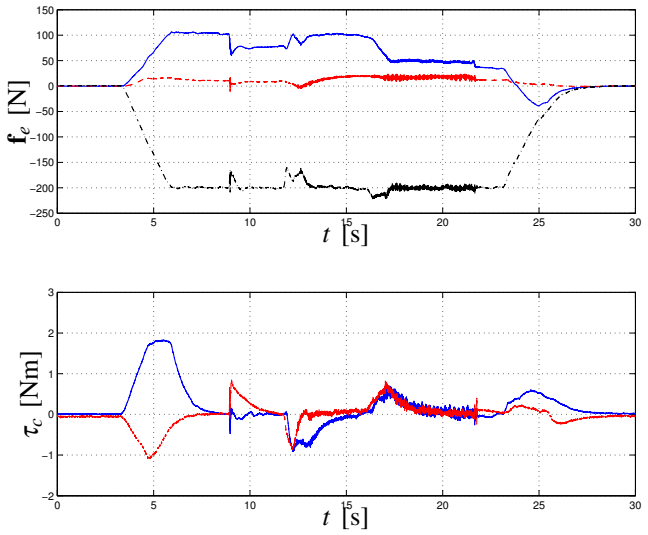

Fig. 5. The forces during a drilling experiment using the built-in motion controllers for the inner-loop control, with no control of the sliding forces. Top: Sliding forces in the x-direction (*solid*) and in the y-direction (*dashed*), and normal (axial) forces (*dash-dotted*). Bottom: Contact moments acting on the TCP point around the x-axis (*solid*) and y-axis (*dashed*). In this case, large tangential forces were built up in the uncontrolled x-direction.

obtained from, e.g., cameras or laser trackers. Here, force measurements and an H_∞-optimal inner controller was designed to give a faster and more decoupled response in contact. The discrete-time robot model obtained from Eq. (6), together with a force sensor low-pass filter, can be written in input-output form

$$\mathbf{p}_a(z) = \mathbf{G}_{ar}(z)\mathbf{p}_r(z) + \mathbf{G}_{af}(z)\mathbf{f}_e(z) \tag{11}$$

$$\mathbf{p}_m(z) = \mathbf{G}_{mr}(z)\mathbf{p}_r(z) + \mathbf{G}_{mf}(z)\mathbf{f}_e(z) \tag{12}$$

$$\mathbf{f}_{e,f}(z) = \mathbf{G}_{LP}(z)\mathbf{f}_e(z). \tag{13}$$

Using the controller

$$\mathbf{p}_r(z) = \mathbf{r}(z) - \underbrace{(\mathbf{C}_m(z)\mathbf{p}_m(z) + \mathbf{C}_f(z)\mathbf{f}_{e,f}(z))}_{\mathbf{v}(z)} \tag{14}$$

the model of the inner loop system was given by

$$\begin{aligned}\mathbf{v} &= (\mathbf{I} + \mathbf{C}_m\mathbf{G}_{mr})^{-1}(\mathbf{C}_m\mathbf{G}_{mf}\mathbf{W}_f\mathbf{f}_e + \mathbf{C}_f\mathbf{G}_{LP}\mathbf{W}_f\mathbf{f}_e + \\ &\quad + \mathbf{C}_m\mathbf{W}_{dm}\mathbf{e}_m + \mathbf{C}_f\mathbf{W}_{df}\mathbf{e}_f) \triangleq \mathbf{G}_v \begin{bmatrix}\mathbf{f}_e^T & \mathbf{e}_m^T & \mathbf{e}_f^T\end{bmatrix}^T \end{aligned} \tag{15}$$

$$\mathbf{p}_a = \mathbf{G}_{af}\mathbf{W}_f\mathbf{f}_e - \mathbf{G}_{ar}\mathbf{v} \triangleq \mathbf{G}_a \begin{bmatrix}\mathbf{f}_e^T & \mathbf{e}_m^T & \mathbf{e}_f^T\end{bmatrix}^T \tag{16}$$

where $\mathbf{e}_f$ and $\mathbf{e}_m$ modeled measurement noise, and the weighting transfer functions $\mathbf{W}_i$ were chosen to give a proper suppression of disturbances $\mathbf{f}_e$ at the arm side position $\mathbf{p}_a$, for frequencies up to approximately 25% of the mechanical bandwidth. This lead to the optimization problem

$$\min_{\mathbf{C}_m,\mathbf{C}_f} \left\| \begin{bmatrix}\mathbf{W}_v\mathbf{G}_v \\ \mathbf{W}_a\mathbf{G}_a\end{bmatrix} \right\|_\infty, \tag{17}$$

which was solved to give the controller transfer functions $\mathbf{C}_m(z)$ and $\mathbf{C}_f(z)$, using standard H_∞-optimization methods [9]. In order to simplify real-time implementation, the high-order controllers obtained were reduced to order 15 using balanced model reduction [9].

The force controller was designed by tuning a desired decoupled impedance in the form

$$\mathbf{M}_I\frac{d^2}{dt^2}\Delta\mathbf{p} + \mathbf{D}_I\frac{d}{dt}\Delta\mathbf{p} = \mathbf{f}_{e,f} - \mathbf{f}_r \tag{18}$$

$$\mathbf{r} = \mathbf{p}_{ref} + \mathbf{K}_{dc}\Delta\mathbf{p} \tag{19}$$

with $\mathbf{M}_I$ and $\mathbf{D}_I$ diagonal matrices. Since the inner loop design was based on a 3-DoF model with translation only, a static decoupling matrix $\mathbf{K}_{dc}$ was included for improved decoupling between the control of xy-torques and xy-forces. A proper choice for $\mathbf{K}_{dc}$ could be found from the static calibration data in Section II. Here, $\mathbf{K}_{dc}$ was chosen such that for all unit basis vectors $\mathbf{e}_i$

$$\Delta\mathbf{p}_{m,i} = \mathbf{K}_{dc}(\mathbf{e}_i^T\Delta\mathbf{p}_{m,i})\mathbf{e}_i \tag{20}$$

where $\Delta\mathbf{p}_{m,i}$ was the motor side motion required for a force change $\Delta f_e\mathbf{e}_i$ in stationarity. The arm side response of the full system to external forces in Fig. 4 was described by the transfer matrix

$$\mathbf{G}_{\text{tot}}(z) = \mathbf{G}_{c,af}(z) + \mathbf{G}_{c,ar}(z)\mathbf{G}_I(z) \tag{21}$$

where $\mathbf{G}_{c,af}(z)$ and $\mathbf{G}_{c,ar}(z)$ were the responses in the tool position $\mathbf{p}_a$ of the closed inner loop to forces $\mathbf{f}_e$ and motion references $\mathbf{r}$, and $\mathbf{G}_I(z)$ represented the discretized dynamics in Eqs. (18)–(19) from applied force to $\mathbf{r}$. The stability of the resulting system could be analyzed by considering a system with $\mathbf{G}_{\text{tot}}(z)$ connected to the environment dynamics in a simple feedback loop.

III. Experiments

The drilling experiments were carried out on an ABB Irb 2400 industrial robot using the external sensor interface described in [4]. The robot was equipped with a pneumatic Atlas Copco LBL25 drilling machine with 4 mm drill diameter. A number of experiments were performed using different robot configurations. The contact forces were measured using a JR3 force/torque sensor, and the workpiece was a 3.5 mm thick plate of high-strength aluminum.

In the first set of experiments, the built-in motion control of the robot was used without force compensation in the inner

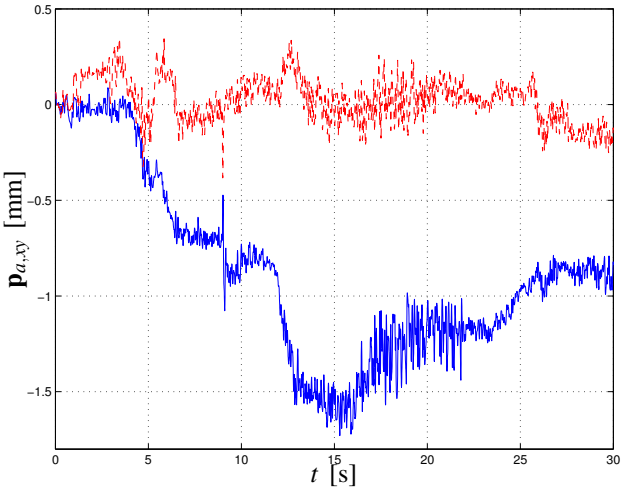

Fig. 6. The linear motion of the tool in the x- and y-directions during a drilling experiment using the built-in motion controllers for the inner-loop control, with no control of the sliding forces. Undesired sliding of around 1.6 mm occurred in the tangential x-direction, caused by the variations in the axial pressure forces.

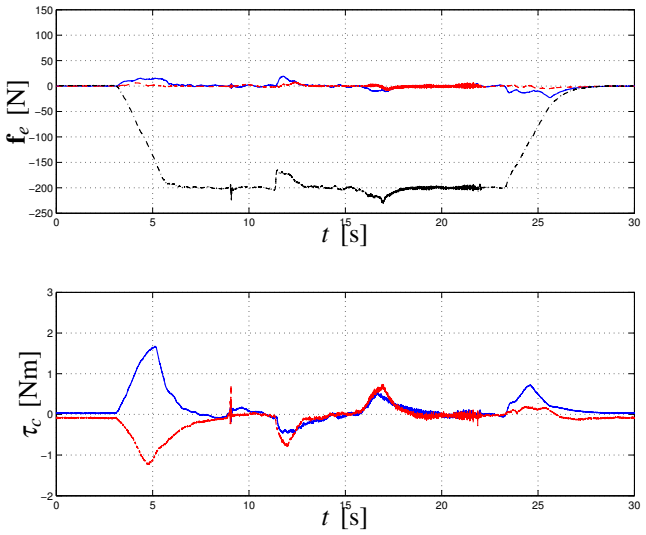

Fig. 7. The forces during a drilling experiment using using an inner-loop controller with compensation for the robot compliance, and with active control of the sliding forces. Top: Sliding forces in the x-direction (*solid*) and in the y-direction (*dashed*), and normal (axial) forces (*dash-dotted*). Bottom: Contact moments acting on the TCP point around the x-axis (*solid*) and y-axis (*dashed*). The tangential forces were controlled to keep the friction contact in the stiction regime.

loop. The axial environment stiffness was approximately 150 N/mm. The approximate stiffness of the robot and tool, with respect to forces applied at the drill tip, was 160 N/mm in the axial z-direction, and 100 N/mm and 50 N/mm in the tangential x- and y-directions. There was also a significant static coupling, resulting in a tangential deflection when axial forces were applied to the drill. In Figs. 5–6 the results from one of the drilling experiments with 3-DoF force/torque control is shown. The axial z-force and the moments around the x- and y-axes were controlled such that a stable contact was achieved with a total axial force of 200 N. However, although the axial force in Fig. 5 was accurately controlled to the desired value, the friction forces between the tripod and the surface were not sufficient to be able to suppress the sliding motion of the tool. This can be seen in Fig. 6, as sliding occurred primarily in the x-direction, both during the application of the pressure foot onto the surface, and when the cutting forces were applied during the drilling. When forces were applied, the tripod contact switched from stiction to slip and back again several times. This behavior is also indicated in Fig. 5, which shows the presence of large x-forces with discontinuities at transitions between stiction and slip. The total deflection in the experiment was approximately 1.6 mm, of which 0.8 mm occurred during the drilling phase. Both the positioning and quality of the resulting holes were unsatisfactory.

In the next set of experiments a 5-DoF force/torque control with an inner-loop force compensation was used, in which the forces in the x- and y-directions were controlled in order to suppress sliding. Figs. 7–8 show the results of a drilling experiment where this controller was used. Except for this change of controller, all other parameters were identical to the previous set of experiments. In Fig. 8 it can be seen that the tool deflection when forces were applied during the force build-up was reduced to approximately 0.1 mm, and sliding during the drilling phase was reduced to

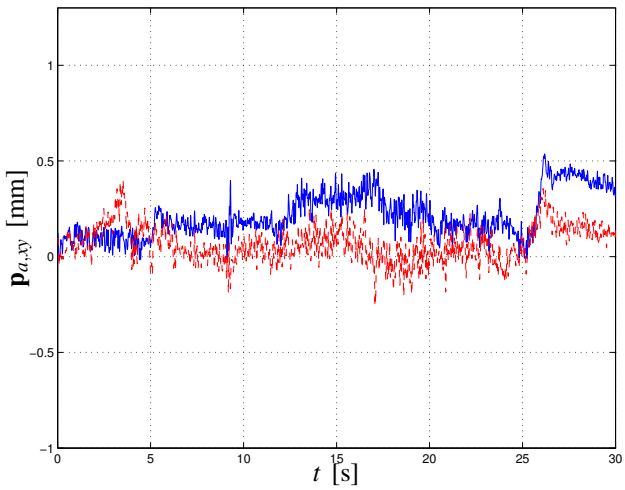

Fig. 8. The linear motion of the tool in the x- and y-directions during a drilling experiment using an inner-loop controller with compensation for the robot compliance, and with active control of the sliding forces. The drill sliding was reduced in the critical drilling phase by a factor of five as compared to the previous case.

0.1 mm. Having performed a number of experiments in different configurations, the model-based force controller was always able to control the sliding forces so that the tripod contact remained in the stiction regime during the entire drilling operation, and the tangential deformation was reduced significantly. More accurate measurements using a 3-DoF Leica laser tracker (Fig. 9), confirmed that the total sliding in the drilling experiments was below 0.2 mm. The Leica laser tracker could also be used to improve the absolute positioning accuracy of the robot, either by robot calibration or by on-line motion corrections.

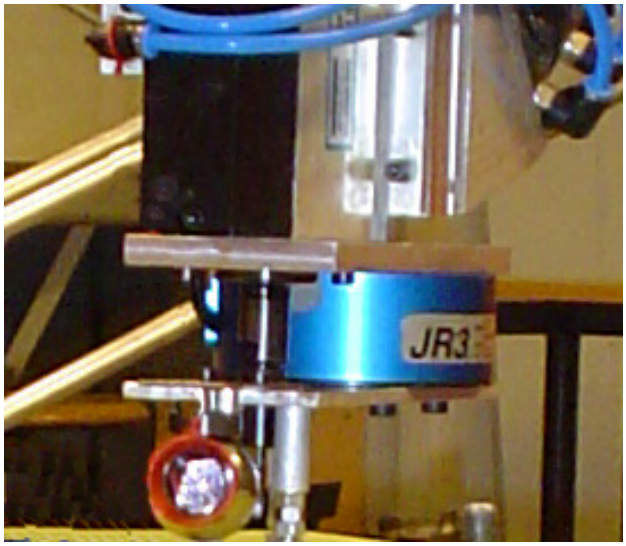

Fig. 9. Drilling tool with attached reflector prism measurement with for Leica laser tracker. The prism was attached to the tripod, giving accurate measurements of the translations at the drill tip.

IV. Discussion

The experiments indicate that the force control of the pressure forces is feasible for drilling tasks. The full 5-DoF force/torque control resulted in greatly improved mechanical stiffness and vibration suppression, leading to significant improvements in hole quality and positioning. The use of an industrial robot and a small tripod also provides good dexterity and flexible usage, making the system operable in a large workspace on complex structures. The use of a tripod limits the system to drilling perpendicularly to the surface, but together with the torque control also helps obtain good normality of the drilled holes.

As an alternative to controlling the position using arm-side position feedback, the controller attempts to achieve sliding suppression by making sure that the tangential interaction forces are always small enough to keep the contact in the stiction regime. In practice, the achievable bandwidth of the force control is limited by the mechanical bandwidth of the robot, as well as by the bandwidth of the inner motion control. Instead, high-frequency disturbances are damped out by of the tripod high-friction contact, providing extra mechanical stiffness against disturbances such as vibrations from the feeding and rotation of the drilling tool. The force control and active sliding suppression takes care of large disturbances at lower frequencies, such as the slower variations of the cutting forces. Thereby, a system which is able to reject disturbances over a wide frequency range is obtained, at a very low cost.

The drilling force control system differs from most other applications of force control, such as polishing, grinding and assembly, where the force control is used to increase the compliance rather than to improve the stiffness to force disturbances. In the drilling system, the model-based inner-loop compensation improves the stiffness, using one or several local models of the robot stiffness and dynamics. In order to experimentally obtain and tune such models, arm side position measurements must be available. In cases when such measurements are not available, acceptable results can in some configurations be obtained without inner loop compensation, using proper tuning of the outer force controller. However, the couplings between different degrees of freedom may lead to poor performance, and attempts to increase the bandwidth may result in limit cycles and oscillations in the force control.

V. Conclusions

The use of industrial robots in automatic drilling applications has been limited, mainly due to the presence of rapidly varying interaction forces in combination with compliance in gear boxes and links. Functionality for high-bandwidth force control in modern industrial robot control systems could potentially lead to robotic drilling systems with significantly improved performance, without the use of costly hardware modifications and calibration procedures. In this paper, we have presented methods and systems for force-controlled robot drilling. Using a 6-DoF force/torque sensor, an outer force control loop and a model-based inner-loop disturbance compensation scheme have been designed, and used to control the axial contact force and suppress the sliding of a tripod contact while the drilling is performed. The advantage of the proposed controller is demonstrated in reproducible drilling experiments using a medium-sized industrial robot system.

VI. Acknowledgements

This work was supported by the Swedish ProViking/SSF project *Flexible and Accurate Automation Using Robot Systems* (FlexAA).

References

[1] S. Kawaji, M. Arao, and Y. Chen, "Thrust force control of drilling system using neural network," in *Proc. IEEE/ASME Int. Conf. Advanced Intelligent Mechatronics*, Como, Italy, 2001, vol. 1, pp. 476–481.

[2] G. Alici, "A systematic approach to develop a force control system for robotic drilling," *Industrial Robot: An International Journal*, vol. 26, no. 5, pp. 389–397, 1999.

[3] W.Y. Lee and C.L. Shih, "Control and breakthrough detection of a three-axis robotic bone drilling system," *Mechatronics*, vol. 16, no. 2, pp. 73–84, 2006.

[4] A. Blomdell, G. Bolmsjö, T. Brogårdh, P. Cederberg, M. Isaksson, R. Johansson, M. Haage, K. Nilsson, M. Olsson, T. Olsson, A. Robertsson, and J. Wang, "Extending an industrial robot controller–Implementation and applications of a fast open sensor interface," *IEEE Robotics and Automation Magazine*, vol. 12, no. 3, pp. 85–94, Sept. 2005.

[5] C. Canudas de Wit, H. Olsson, K.J. Åström, and P. Lischinsky, "A new model for control of systems with friction," *IEEE Trans. Automatic Control*, vol. 40, no. 3, pp. 419–425, 1995.

[6] N. Diolaiti, C. Melchiorri, and S. Stramigioli, "Contact impedance estimation for robotic systems," *IEEE Trans. Robotics*, vol. 21, no. 5, pp. 925–936, 2005.

[7] J. Park and K Khatib, "Multi-link multi-contact force control for manipulators," in *Proc. IEEE Int. Conf. Robotics and Automation*, Barcelona, Spain, April 2005, pp. 3624–3629.

[8] C. Natale, R. Koeppe, and G. Hirzinger, "A systematic design procedure of force controllers for industrial robots," *IEEE/ASME Trans. Mechatronics*, vol. 5, no. 2, pp. 122–131, 2000.

[9] K. Zhou and J.C. Doyle, *Essentials Of Robust Control*, Prentice Hall, Upper Saddle River, NJ, 1998.